Materials Research Express

PAPER • **OPEN ACCESS**

Effect of Gd^{3+} substitution on proton relaxation and magnetic hyperthermia efficiency of cobalt ferrite nanoparticles

To cite this article: Jaison D *et al* 2020 *Mater. Res. Express* **7** 064009

Materials Research Express

PAPER

Effect of Gd^{3+} substitution on proton relaxation and magnetic hyperthermia efficiency of cobalt ferrite nanoparticles

Jaison D[1], **Meher Abhinav E**[1], **Asnit Gangwar**[2], **Prasad Nand Kishore**[2], **Gopalakrishnan Chandrasekaran**[3,5] and **Mothilal M**[4,5]

[1] Nanotechnology Research Centre, SRM Institute of Science and Technology, Kattankulathur, Tamil Nadu, 603203, India
[2] Department of Metallurgical Engineering, Indian Institute of Technology (BHU), Varanasi, 221005, India
[3] Department of Physics and Nanotechnology, SRM Institute of Science and Technology, Kattankulathur, Tamil Nadu, 603203, India
[4] Department of Pharmaceutics, SRM College of Pharmacy, Kattankulathur, Tamil Nadu, 603203, India
[5] Authors to whom any correspondence should be addressed.

E-mail: mothipharma78@gmail.com **and** cgknano@gmail.com

Keywords: cobalt ferrite (CF), gadolinium substituted cobalt ferrite nanoparticles (CFG), proton relaxation, magnetic hyperthermia

OPEN ACCESS

RECEIVED
5 March 2020

REVISED
24 April 2020

ACCEPTED FOR PUBLICATION
15 May 2020

PUBLISHED
17 June 2020

Abstract

In this study, Gadolinium substituted Cobalt Ferrite nanoparticles ($CoFe_{2-x}Gd_xO_4$, $0 \leqslant x \leqslant 0.4$) were prepared via hydrothermal route using triethylamine as reducing agent at 180°C for 12 h. X-ray diffraction studies revealed the single phase cubic spinel structure for both Cobalt ferrite (CF) and Gadolinium substituted Cobalt Ferrite (CFG) nanoparticles ($x \leqslant 0.24$). An increase in the Specific absorption rate (SAR) was observed with increase in Gd concentration. Further with increase in the molar concentration ($x > 0.24$), gadolinium hydroxide was observed as the secondary phase, which was also confirmed by the Gd–O stretching vibrations observed in Fourier transform Infrared spectroscopy. The evolution of Gadolinium hydroxide showed a strong influence in the relaxivity (r_1) and hyperthermia potential. Field emission scanning electron microscopy revealed that CF and CFG ($x \leqslant 0.24$) nanoparticles were spherical in nature with particle size ranging from 10 to 25 nm, whereas the particle size increases above 30 nm for CFG ($0.3 \leqslant x \leqslant 0.4$) nanoparticles along with the presence of columnar shaped particles. Magnetic measurements confirmed the pseudo single domain, ferrimagnetic nature of CF and CFG nanoparticles. The magnetization data revealed a change in direction of magnetization towards easy axis with increasing Gd concentration. The orientation of magnetization direction towards easy axis had induced change in the hyperthermia potential. Proton relaxation studies of CF and CFG nanoparticles revealed that there is a strong interaction between the relaxivities r_1 and r_2. The specific absorption rate of CF and CFG nanoparticles were observed to be in the range from 91.49 W g^{-1} to 232.17 W g^{-1} at applied Hf of 4.19×10^9 Am^{-1} s^{-1}.

Introduction

The concept of hyperthermia was originated and been in practice over several centuries by ancient Greeks, Romans and Egyptians for the treatment of breast cancer [1–3]. However the acceptance of hyperthermia as a treatment for cancer has been seriously considered only in the 20th century after its successful clinical trials [3]. The spatial control in heating of biological tissue remains a challenge with various physical mechanisms such as microwave irradiation, ohmic heating, optical laser irradiation and whole body hyperthermia (water bath heating) [4]. Magnetic nanoparticle hyperthermia has gained its special attention due to their ability to concentrate the heat in the specific target area without affecting the other biological tissues [5–7]. Magnetic nanoparticles also play a significant role in the other biomedical fields such as magnetic resonance imaging (MRI) [8, 9], targeted drug delivery systems [10–12], tissue engineering [13–15], labelling and separation of cells [16] and proteins [17, 18] and integrated lab on chip technology for monitoring, diagnosis and therapy [19, 20]. The contrasting ability, high magnetic moment and heating ability of magnetic materials makes them an ideal candidate for theragnostic applications.

Among the magnetic materials, spinel ferrites were attracted by various researchers because of their thermal and chemical stability [21]. Several methods such as Co-precipitation [22], Sol-gel [23], thermal decomposition [24], non-aqueous synthesis [25], Micro-wave assisted [26], polyol [27], sonochemical [28], microemulsion [29] and hydrothermal [30] have been adopted for the synthesis of ferrites with different morphologies for various applications, of which the latter delivers a control over morphology, composition, particle size distribution and aggregation [30–32] through regulation of rate and uniformity of nucleation [33].

The translation of magnetic hyperthermia into a standard medical procedure requires an improvement in successful administration of nanoparticles into the intra-tumoural region, reaching and maintaining the therapeutic temperature inside the tumour tissue [4, 34]. The heating of magnetic materials occurs through Neel and Brownian relaxation losses in superparamagnetic and hysteresis losses in ferri/ferro magnetic materials [3, 35, 36]. The heating potential of superparamagnetic materials rely only on Neel relaxation as different biological tissues have different viscosities, leading to the loss of Brownian relaxation [3, 37]. Whereas, the ferri/ferro magnetic materials requires application of high magnetic field, frequency and power to achieve increased specific absorption rate [38, 39], which is clinically not realisable due to physiological constraints [3]. After various experiments, the maximum threshold of *Hf* factor for hyperthermia application was estimated to be $5 \times 10^9\ \mathrm{Am^{-1}\ s^{-1}}$ to avoid any detrimental effects on healthy tissues due to electromagnetic radiation exposure [40]. The materials should be able to achieve therapeutic heat dose at low applied magnetic field to overcome the physiological constraints. Hergt *et al* suggested that high specific absorption rate (SAR) value can be achieved with the particles whose size is near the transition from superparamagnetic to ferromagnetic behaviour [41]. Rumenapp and his coworkers reported that the magnetic resonance imaging capability of the super-paramagnetic and ferromagnetic materials were almost equal [42].

Though there are several reports available related to hyperthermia, the region between single domain and multi-domain ferromagnetic nature of nanomaterials were not investigated till date. Hence, there is a vast scope in developing manifold magnetic nanoparticles with high SAR to work in the therapeutic region. In this study, the effort has been made to develop a Pseudo domain ferrimagnetic nanomaterial with better contrasting ability and high SAR suitable for theragnostic applications.

Materials and method

$CoFe_{2-x}Gd_xO4$ was prepared using Hydrothermal method by dissolving 10 mM Cobalt Nitrate, (20-x) mM Ferric Nitrate and 'x' mM Gadolinium Acetate (where, $x = 0$ (CF), 0.04 (CFG02), 0.08 (CFG04), 0.12 (CFG06), 0.16 (CFG08), 0.20 (CFG10), 0.24 (CFG12), 0.30 (CFG15) and 0.40 (CFG20)) in 60 ml of aqueous media. The aqueous solution was titrated with 10% Triethylamine until pH 10.5 was reached. The reaction mixture was enclosed in 100 ml Teflon coated autoclave and kept at 180 °C for 12 h. The autoclave was allowed to cool to room temperature gradually. Dark brown precipitate was obtained, which was further washed with DI water multiple times and ethanol, air dried at 60 °C overnight.

The structural properties of the CFG nanoparticles were characterized by PANalytical Xpert Pro x-ray diffraction system (XRD) with Cu-kα source. The morphological characters such as particle shape and size was studied using Field Emission Scanning electron Microscopy (FESEM), FEI Quanta, USA. The Elemental composition was detected using Energy Dispersive Spectroscopy (EDS), Bruker, Germany at an accelerating voltage of 20 KV for samples $0 \leqslant x \leqslant 0.24$ and 30 KV for samples $x = 0.3$ and 0.4. The vibrational frequencies of oxides and other organic impurities were studied using Fourier transform infrared spectroscopy (FTIR). Magnetization measurement of the CF and CFG nanoparticles was carried out using Vibrating Sample Magnetometer (VSM), Lakeshore, USA. The T_1 and T_2 relaxation times were measured using Minispec benchtop Time domain NMR Spectrometer, Bruker, Germany, equipped with a 470 mT (20.00 MHz for 1 H) permanent magnet. The T_1 relaxivity (r_1) of the nanoparticles were found from the slope of line fitted to $1/T_1$ versus Gd concentration in milli Moles (mM) whereas T_2 relaxivity (r_2) was obtained from the slope of $1/T_2$ versus Fe concentration in mM. The hyperthermic potential of the nanoparticles were measured under AC magnetic field at a frequency of 150 KHz and 35 mT with the help of 30 mm heating coil using MSI Automation Inc., USA equipped with Neoptix fiber sensor system. The specific absorption rate of CF and CFG nanoparticles were calculated from the data obtained from the hyperthermia potential by using initial slope method using the formula,

$$SAR = \frac{Cw\ Ms}{Mm} \times \frac{dT}{dt}$$

Where Cw is the specific heat capacity ($4.187\ \mathrm{Jg^{-1}\ K^{-1}}$) of water, Mm and Ms are the mass of nanoparticles alone and nanoparticles along with dispersion medium respectively, dT/dt is the rate of change of temperature with respect to time.

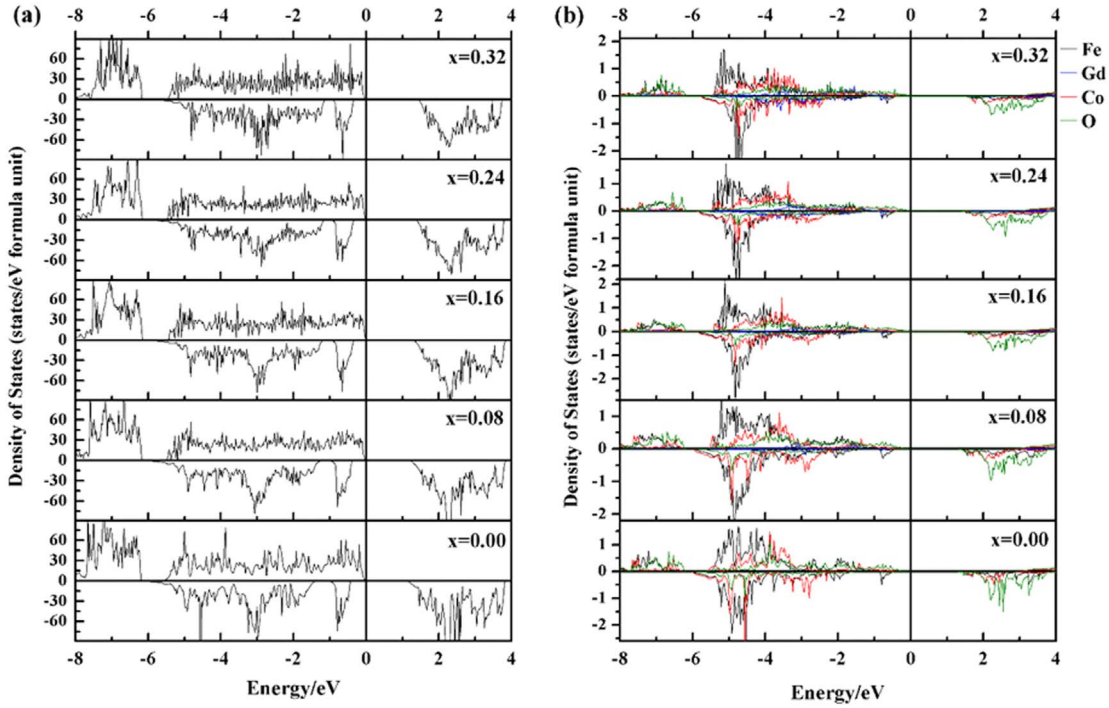

Figure 1. (a) Total density of states, (b) Density of states of individual atoms.

The structural, magnetic and electronic properties of both Cobalt ferrite (CF) and Gadolinium substituted Cobalt ferrite (CFG) were also calculated theoretically using density functional theory (DFT). The Structure optimization, magnetic and electronic calculations were performed using Vienna *Ab initio* simulation package (VASP). The cutoff energy of 520 eV with $5 \times 5 \times 5$ K-mesh was used for optimization calculations and tetrahedron method with $9 \times 9 \times 9$ K mesh was used for total energy calculations. The generalized gradient approximation GGA + U approach has been applied for all the calculations. We applied $U = 4.06$ eV, $J = 0.80$ eV for Co and $U = 4.19$ eV and $J = 0.81$ eV for Fe. The magnetic moments in octahedral and tetrahedral sites are maintained antiparallel in both the structures.

Results and discussion

The total density of states (TDOS) of cobalt ferrites (CF) and gadolinium substituted cobalt ferrites (CFG) using GGA+U are shown in the figure 1(a). The crystal field (cf) theory states that in tetrahedral site of cobalt ferrites, the e_g levels are lower than the t_{2g} levels due to the direct electrostatic repulsion between d_{xy}, d_{yz} and d_{zx} orbitals and surrounding anion orbitals, while in octahedral sites the order is reversed as the d_{z2} and d_{x2-y2} orbitals are repelled directly. The relative strength of crystal field and intra-atomic exchange field (ef) determine the possible high spin (cf $<$ ef) or low spin (cf $>$ ef) electronic configurations [43]. From the TDOS, the band gap of the cobalt ferrite widens as the substitution of gadolinium increases from 1.58 eV to 1.68 eV. This can be explained by Burstein-Moss effect, wherein it states that the increase in the doping concentration in case of n type dopant, the electrons populates within the conduction band moves the fermi level to higher energy [44]. The density of states of individual atoms (figure 1(b)) indicates that the electrons in the atoms becomes localized with the increase in the doping of gadolinium. The localization of electrons was also evidenced by the decrease in the charge density from 418.80 to 402.79 Coulombs/meter^3. This decrease in the charge density also indicates the decrease in bond strength and increase in distance between the atoms due to the introduction of gadolinium in to the lattice whose ionic radii is comparatively larger than the iron. This increase in the bond length decreases the overlapping of electrons from different atoms leading to an increase in their band gap.

The x ray Diffraction studies (figure 2(a)) showed a single phase cubic spinel (Fd -3m) structure of cobalt ferrite (JCPDS # 022-1086) for CF and CFG nanoparticles with $0 \leqslant x \leqslant 0.24$. Hexagonal phase Gadolinium hydroxide (CIF#4031383) with space group P 63/m was observed as a secondary phase with the increase in molar concentration ($x > 0.24$). The lattice constant of inverse spinel CF and CFG nanoparticles were determined by theoretical (VASP) and experimental (High score Plus) data and the values are depicted in the figure 2(b). Both theoretical and experimental values showed an increase in lattice parameters from 8.5677 Å to

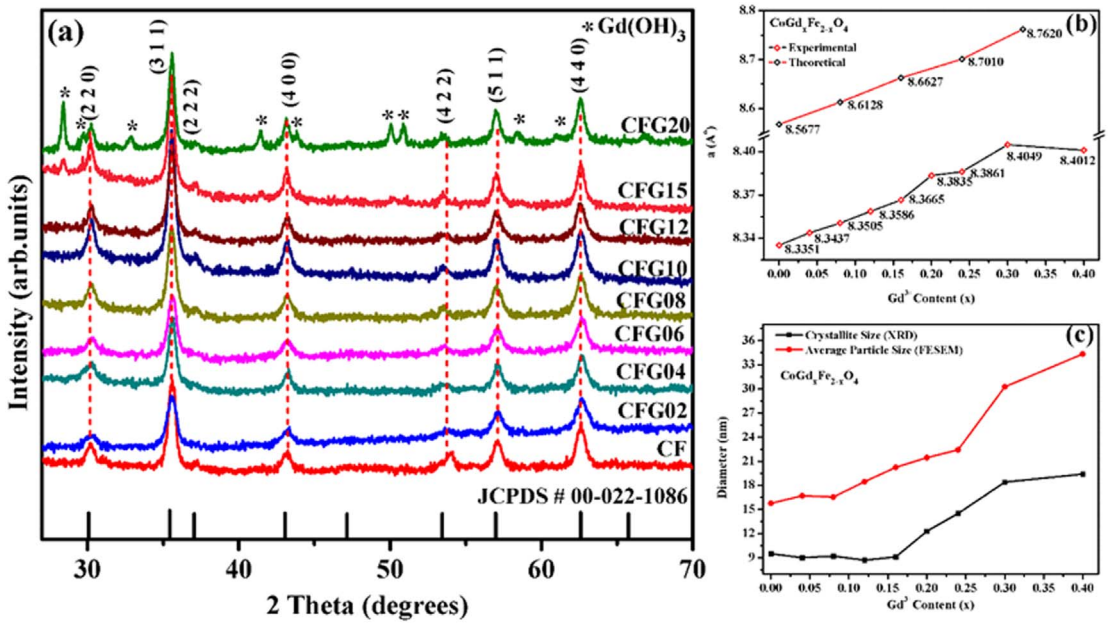

Figure 2. (a) XRD pattern, (b) Lattice constant, (c) Crystallite size and Particle size of $CoGd_xFe_{2-x}O_4$ nanoparticles.

8.7620 Å and 8.3351 Å to 8.4049 Å respectively with the increase in gadolinium concentration ($0.0 \leqslant x \leqslant 0.3$). From theoretical calculations it was found that the lattice constant 'b' is 8.7105 and 8.7585 for 12% and 16% doping of gadolinium in cobalt ferrite which is comparatively lesser than 'a' and 'c' (where $a = c$). The change in the lattice constant 'b' indicates the increased strain in the lattice, which is evidenced by the origination of the secondary phase gadolinium hydroxide. The crystallite size of gadolinium substituted cobalt ferrites ($0.0 \leqslant x \leqslant 0.4$) calculated using Williamson hall (WH) plot was recorded in the figure 2(c). It was observed that the crystallite size does not change appreciably with the increased substitution of gadolinium concentration ($0.0 \leqslant x \leqslant 0.16$). Further increase in the gadolinium concentration ($0.2 \leqslant x \leqslant 0.4$) substantially increases the crystallite size. The increase in lattice constant and crystallite size of gadolinium substituted cobalt ferrites ($0.0 \leqslant x \leqslant 0.3$) was greatly influenced by the substitution of Gd^{3+} (94 pm), a larger ionic radii in the place of smaller Fe^{3+} (67 pm) ions. A higher concentration of Gd^{3+} ($x > 0.3$) substitution exhibits a reverse trend in lattice parameter, which may be attributed to the saturation limit of Gd^{3+} in Cobalt ferrite lattice. The trend of lattice constant also explains the incorporation of Gd^{3+} ions into the interstitial sites at lower concentrations, whereas at the higher concentration segregation or accumulation of Gd^{3+}on the surface takes place distorting the Cobalt ferrite lattice. The lattice strain of CF, CFG02, CFG04, CFG06, CFG08, CFG10, CFG12, CFG15, CFG20 nanoparticles obtained by WH plot were −0.2, −0.1, −0.1, −0.1, 0, 0, 0.1, 0.2, 0.2 respectively. The induction of lattice strain in the crystal structure was directly proportional to the increase in lattice parameter and crystallite size, which was greatly influenced by the higher gadolinium concentration in the parent cobalt ferrite.

The FESEM images of the synthesized CF and CFG nanoparticles were shown in figure 3. It was observed that CF and CFG ($0.04 \leqslant x \leqslant 0.24$) nanoparticles were uniform, slightly aggregated and almost spherical in shape. Beyond $x \geqslant 0.3$ a columnar shaped particles (ranges from 0.4 to 1.0 μm in length) indicating the emergence of hexagonal gadolinium hydroxide along with the spherical particles was observed. The particle size and the size range was measured by using the image J software. The average particle size of the CF and CFG nanoparticles were shown in the figure 2(c). The particle size ranges form 9–20 nm, 11–24 nm, 10–21 nm, 12–25 nm, 15–24 nm, 16–26 nm, 16–30 nm, 24–32 nm, 27–44 nm for CF, CFG02, CFG04, CFG06, CFG08, CFG10, CFG12, CFG15, CFG20 nanoparticles respectively. The particle size monotonically increase with increase in the concentration of gadolinium, which is further explained by the substitution of larger ionic radii of Gd^{3+} at Fe^{3+} ionic site. The increasing trend of particle size observed by FESEM are in good agreement with the crystallite size obtained from the XRD data.

The energy dispersed along with molecular weight percentage and atomic weight percentage of CF and CFG nanoparticles were shown in EDS (figure 4). The ratio of molar concentration of the CF and CFG nanoparticles synthesized was 1:(2-x):x:4 (Co:Fe:Gd:O). Elemental analysis revealed that the Gd/Fe ratio in CF and CFG nanoparticles are in good agreement with the theoretical ratio of the synthesized nanomaterials except with the samples CFG15 and CFG20 as shown in the table 1. The atomic percentage of the oxygen detected in all the

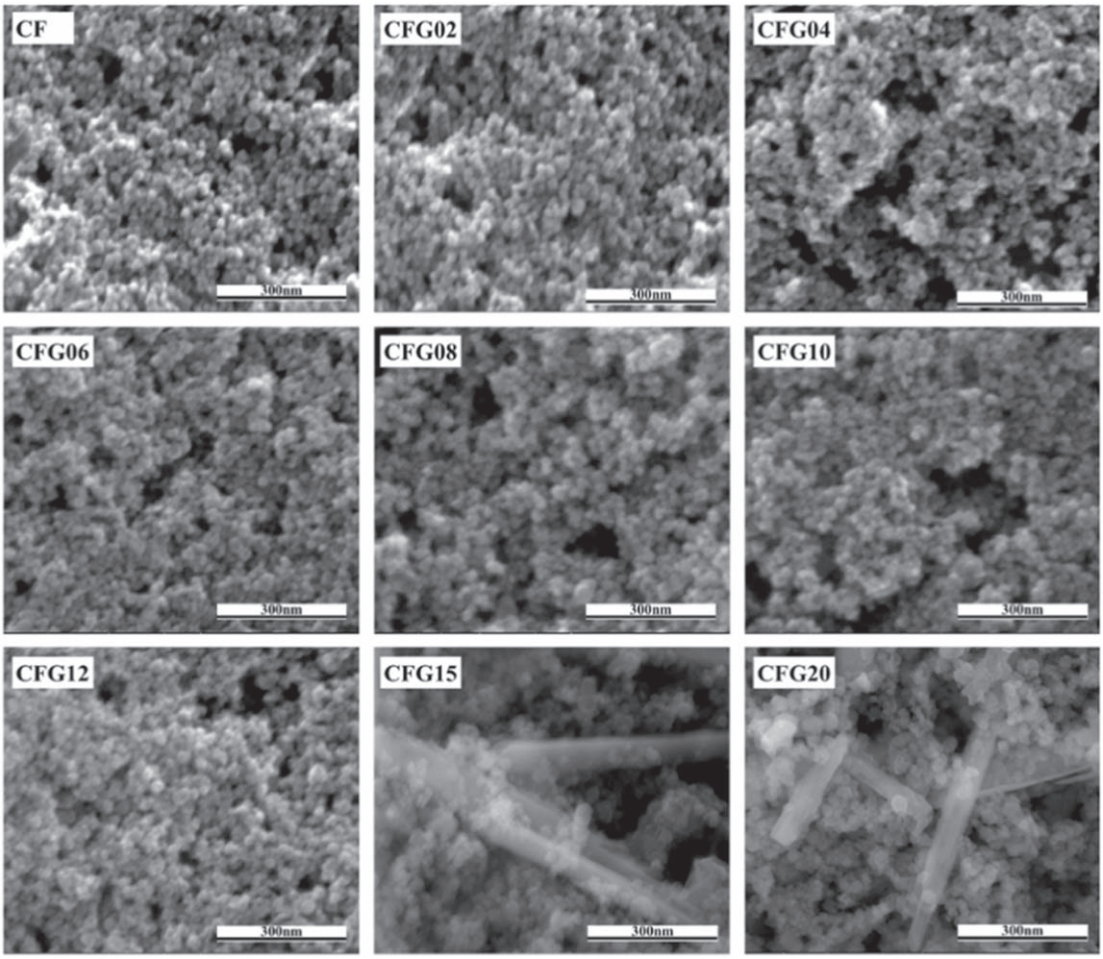

Figure 3. FESEM of $CoGd_xFe_{2-x}O_4$ nanoparticles.

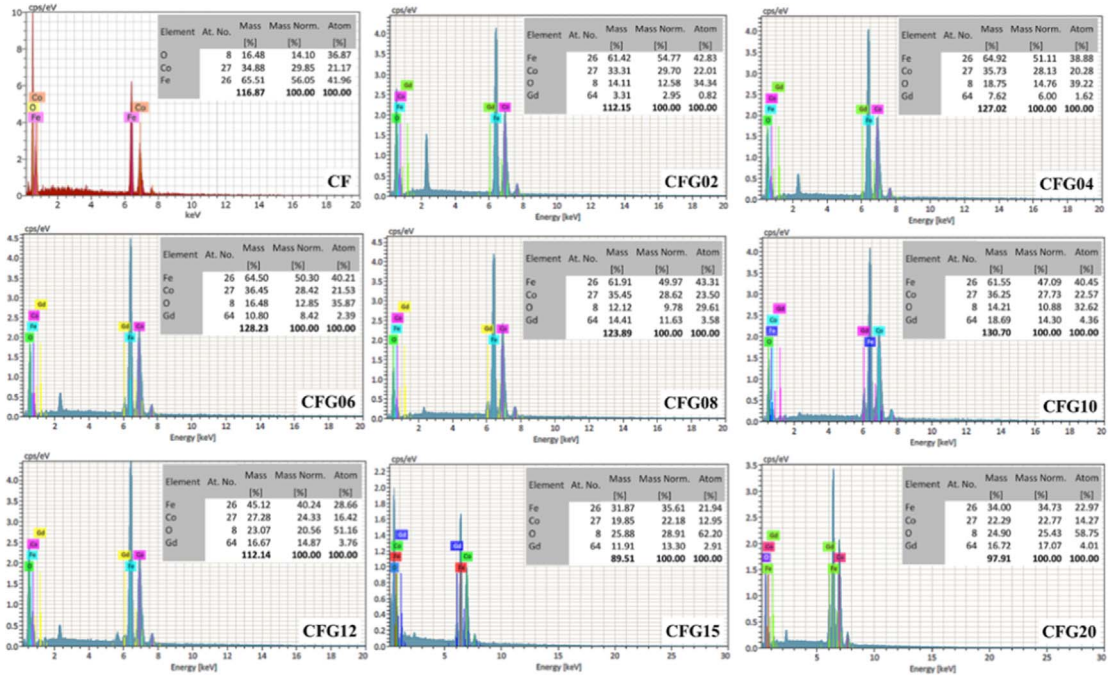

Figure 4. EDS of $CoGd_xFe_{2-x}O_4$ nanoparticles.

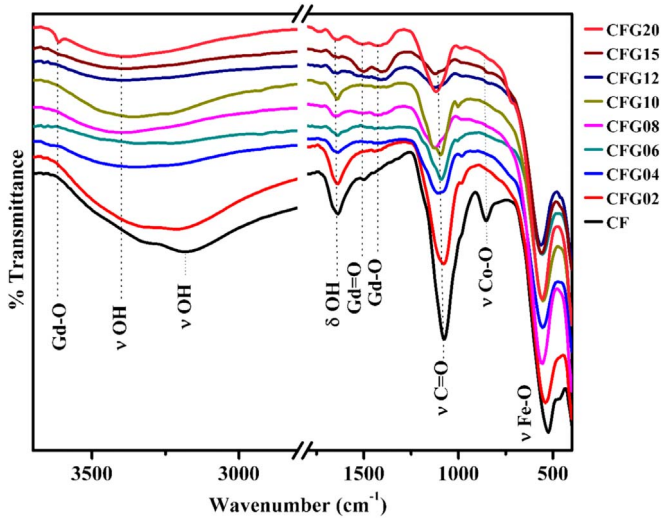

Figure 5. FTIR of $CoGd_xFe_{2-x}O_4$ nanoparticles.

Table 1. Elemental molar composition of CF and CFG nanoparticles.

					Gd/Fe	
Sample code	Co	Fe	Gd	O	Theoretical	Experimental
CF	1.000	1.9816	0.000	1.7408	0	0
CFG02	1.000	1.9462	0.0372	1.8774	0.0204	0.0191
CFG04	1.000	1.9175	0.0799	1.9338	0.0417	0.0417
CFG06	1.000	1.8678	0.1110	1.666	0.0638	0.0594
CFG08	1.000	1.8426	0.1523	1.2594	0.0869	0.0826
CFG10	1.000	1.7921	0.1933	1.4460	0.1111	0.1079
CFG12	1.000	1.7454	0.2290	3.114	0.1364	0.1312
CFG15	1.000	1.6943	0.2247	4.804	0.1765	0.1326
CFG20	1.000	1.6096	0.2809	4.1160	0.2500	0.1745

samples varied substantially than the expected atomic percentage for CF and CFG ($0.04 \leqslant x \leqslant 0.24$) nanoparticles. The profound variation of oxygen is mainly due to low accelerating voltage (20 KV) used for analysis with or without the combined effects such as formation of more favorable auger electrons compared to the less favorable x-rays, low fluorescence yield, inability of low energy x-rays to leave the sample, absorption of photons in certain regions of detector and peak overlapping with L, M, N lines of heavier elements [45]. From the elemental analysis of CF and CFG ($0.04 \leqslant x \leqslant 0.4$) nanoparticles, it is clearly evident that various concentrations of gadolinium is incorporated into cobalt ferrite.

The chemical nature and presence of organic impurities in the synthesized CF and CFG nanoparticles was further confirmed from the vibrational frequencies obtained by FTIR spectroscopy (figure 5). The vibrational frequencies of CF and CFG nanoparticles were depicted in the table 2. Parent cobalt ferrite was confirmed by the presence of a strong characteristic band for Co–O stretching (850.61 cm^{-1}) and Fe–O stretching (532.29 cm^{-1}) vibrations [46, 47]. The substitution of the gadolinium in the parent cobalt ferrite was clearly evident with the emergence of additional stretching vibrations at the region of ~1400 cm^{-1} corresponding to the Gd–O linkage for CFG ($0.04 \leqslant x \leqslant 0.4$) nanoparticles [48]. It was also found that the substitution of gadolinium over $x \leqslant 0.3$ showed a characteristic vibrational frequency of Gd=O linkage and Gd–O–H linkage at the region of ~1500 cm^{-1} and ~3610 cm^{-1} [48, 49]. The vibrations at the region of ~1400 cm^{-1}, ~1500 cm^{-1} and ~3610 cm^{-1} corresponding to Gd–O, Gd=O, Gd–O–H linkages confirm the presence of Gadolinium hydroxide and are in good agreement with the XRD results. All the synthesized samples exhibits strong reflections corresponding to the C=O stretching (~1090 cm^{-1}), O–H bending (~1640 cm^{-1}) and O–H (~3350 cm^{-1}) stretching confirm the presence of COOH functional group which might have been arisen during synthetic process. A shift in the frequency towards the higher wavenumber was observed for the Co–O, Fe–O, C=O and O–H stretching vibrations. This shift in the wavenumber towards higher frequencies for CFG ($0.04 \leqslant x \leqslant 0.24$) could be either due to decrease in the bond length which may be further due to the influence of hydrogen bonding by COOH functional moiety and/or may be due to the overlapping of interstitial Gd-O

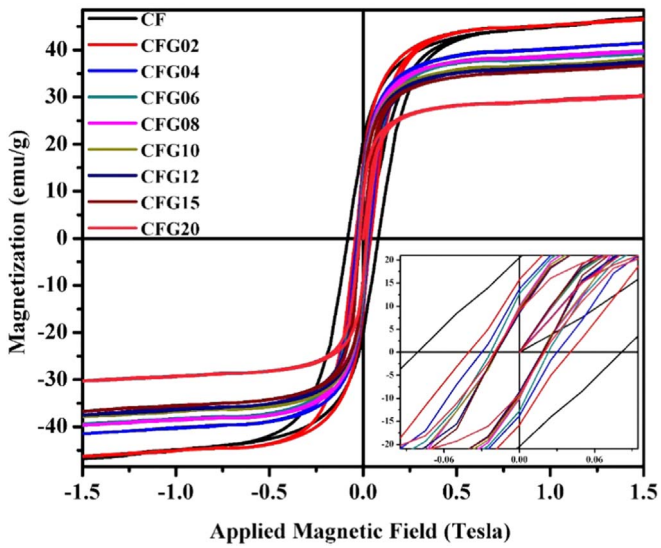

Figure 6. M–H curve of $CoGd_xFe_{2-x}O_4$ nanoparticles.

Table 2. Vibrational frequencies of $CoGd_xFe_{2-x}O_4$ nanoparticles.

Sample code	υCo–O (cm^{-1})	υFe–O (cm^{-1})	υC=O (cm^{-1})	δOH–O (cm^{-1})	υOH–O (cm^{-1})	Gd–O (cm^{-1})	Gd=O (cm^{-1})
CF	850.61	532.29	1067.75	1640.16	3184.52	—	—
CFG02	858.39	541.78	1073.78	1640.16	3210.79	1405.82	—
CFG04	864.81	553.81	1099.39	1644.98	3363.44	1404.24	—
CFG06	856.19	555.13	1093.61	1638.21	3288.28	1403.56	—
CFG08	871.12	559.86	1122.93	1649.10	3395.19	1403.41	—
CFG10	880.81	553.80	1093.95	1639.53	3374.24	1402.21	—
CFG12	878.93	565.31	1124.63	1646.08	3396.58	1403.16	—
CFG15	844.96	559.86	1129.87	1641.36	3381.14	1407.83 3611.14[a]	1502.18
CFG20	844.12	559.14	1119.92	1645.19	3385.22	1415.93 3613.20[a]	1514.39

[a] Gd–O–H stretching vibration.

vibrations (525 cm^{-1} and 835 cm^{-1}) with Co–O and Fe–O stretching vibrations. The frequency shift to lower wavenumber was observed for Co–O and Fe–O stretching in CFG ($0.3 \leqslant x \leqslant 0.4$) nanoparticles due to decreased overlapping of vibrational frequencies, as at higher concentration segregation of Gd^{3+} ions takes place. The wavenumber of Gd–O (~1400 cm^{-1}) remains constant for CFG ($0.04 \leqslant x \leqslant 0.24$) nanoparticles, whereas the shift to higher wavenumber is observed in CFG ($0.3 \leqslant x \leqslant 0.4$) due to the emergence of the gadolinium hydroxide as an impurity phase.

The room temperature hysteresis of the CF and CFG nanoparticles was recorded using vibrating sample magnetometer at applied field from −1.5 to +1.5 tesla. Figure 6 indicates the ferri-magnetic nature of the particles and also revealed a slight shift in the magnetization direction from hard axis to easy axis. The ferri-magnetic behavior is observed when the magnetic moment of the sample interacts with the super exchange interactions [50]. The magnetic saturation of the CF and CFG nanoparticles were determined by using law of approach [51] and are represented in the table 3. The magnetic remanance (Mr) and magnetic saturation (Ms) were found to decrease with an increase in the gadolinium concentration. An abrupt decline in Ms beyond $x \geqslant 0.3$ is majorly due to the presence of paramagnetic gadolinium hydroxide, which has contributed to the total net magnetization of the CFG nanoparticles. The coercivity of the Cobalt ferrite decreases upto $x \geqslant 0.2$ and then increases slightly upon further doping. Similarly the anisotropy constant was found to decrease with increase in gadolinium concentration mainly due to the magnetic distortion, weak coupling to crystal structure, weak interaction of Fe–Re. The Mr/Ms and Hr/Hc values indicate that CF and CFG nanoparticles represent pseudo single domain characteristics [52]. It was also observed both theoretically and experimentally that the

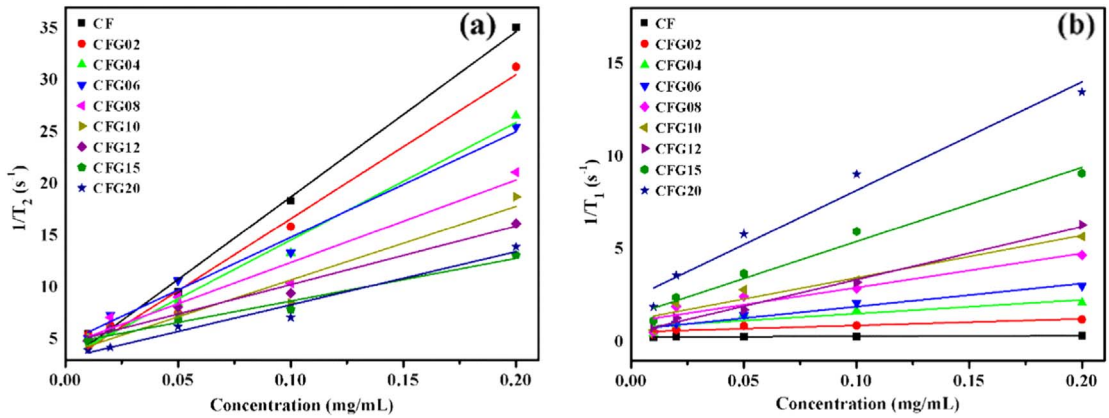

Figure 7. Plots of (a) $1/T_2$ relaxation as a function of Fe concentration, (b) $1/T_1$ relaxation as a function of Gd concentration.

Table 3. Magnetic properties of CF and CFG nanoparticles.

							Bohr magneton (μ_B)		
Sample code	Hc	Mr	Ms	Hr	Mr/Ms	Hr/Hc	Theoretical	Experimental	Anisotropic constant
CF	0.0813	20.480	48.286	0.177	0.424	2.181	1.8022	2.03	202 346.10
CFG02	0.0408	15.755	47.324	0.101	0.333	2.482	—	2.02	99 966.73
CFG04	0.0300	13.787	42.513	0.073	0.324	2.416	1.7153	1.85	65 920.44
CFG06	0.0231	12.532	40.064	0.066	0.313	2.880	—	1.77	47 653.77
CFG08	0.0178	10.112	40.499	0.064	0.249	3.567	1.6284	1.82	37 168.67
CFG10	0.0181	9.649	38.432	0.072	0.251	3.989	—	1.75	35 717.84
CFG12	0.0184	8.553	38.244	0.050	0.224	2.743	1.4726	1.77	36 087.61
CFG15	0.0188	9.117	37.490	0.055	0.243	2.906	1.4548[a]	1.78	36 363.06
CFG20	0.0199	9.079	30.803	0.066	0.295	3.300	—	1.52	32 945.60

[a] 16% Gadolinium doped Cobalt ferrite.

magnetization and bohr magneton (μB) decreases with increase in Gd concentration. The difference in the bohr magneton value could be due to the magnetic interactions due to random occupation of the Fe sites by the gadolinium. The crystalline symmetry of nanoparticles was reduced with the strain in lattice with doping. The decrease in the magnetic saturation, magnetic anisotropy and coercivity is mainly due to the random occupation of dopant atoms in substitutional positions. In pristine cobalt ferrite, the magnetic interactions are high thus leading high coercivity and magnetic retentivity.

Proton relaxation studies

Different concentration (0.0 to 0.2 mg) of CF and CFG nanoparticles in 0.05% w/v poly acrylic acid (PAA) gel were studied for the T_1 and T_2 relaxation rates at room temperature. Both T_2 and T_1 relaxation rates depicted in the figures 7(a) and (b) clearly showed that they are highly dependent on the concentration of the Iron and Gadolinium respectively. The r_1 and r_2 proton relaxivity values obtained from the slope of line fitted to the $1/T_1$ *versus* Gd concentration and $1/T_2$ versus Fe concentration respectively were tabulated in the table 4. It was found that the relaxation rate ($1/T_2$) and relaxivity (r_2) decreases with increase in the Gd concentration until $x \leqslant 0.24$. The decrease in relaxivity (r_2) can be due to decreasing saturation magnetization, as the magnetic moment of Gd is anti-parallel and their increased concentration opposes the net magnetic moment induced by Fe-Fe interaction [53]. Whereas, the increase in relaxivity was observed with Gd ($x \geqslant 0.3$) due to the evolution of gadolinium hydroxide. The T_1 relaxation rate and relaxivity (r_1) of pure cobalt ferrite nanoparticles remains negligible, whereas it gradually increases with increasing concentration of the Gadolinium. The gradual rise in relaxivity (r_1) is mainly due to induced signal reduction of T_2 which is further due to weak Re–Fe interactions [53]. The samples CFG15, CFG20 showed a sudden increase in relaxivity (r_1) as the Gd^{3+} ions are densely populated due to the occurrence of gadolinium hydroxide as a secondary phase. The abrupt rise in relaxivity (r_1) with respect to decreased Iron concentration and evolution of gadolinium hydroxide clearly states that Iron quenches the T_1 relaxivity of Gadolinium in cobalt ferrites.

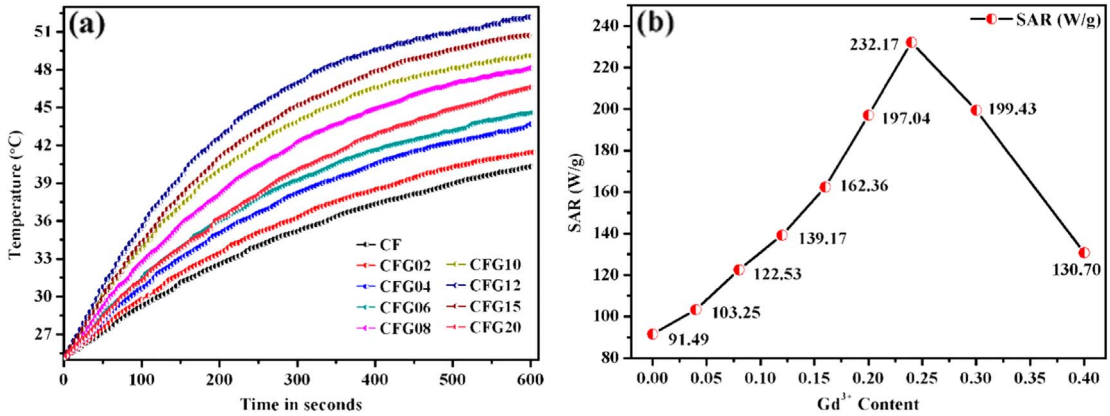

Figure 8. Plots of (a) Temperature dependence on Time, (b) Specific absorption rate.

Table 4. Relaxation efficiency of CF and CFG nanoparticles.

Sample code	r_1 Proton relaxivity ($mM^{-1}\ s^{-1}$)	r_2 Proton relaxivity ($mM^{-1}\ s^{-1}$)
CF	Negligible	79.1756
CFG02	34.4474	72.9319
CFG04	35.3728	62.4327
CFG06	44.8915	59.5883
CFG08	45.7807	48.7471
CFG10	44.2851	46.0576
CFG12	48.6034	38.7572
CFG15	80.6061	30.6547
CFG20	98.3190	43.2538

The hyperthermia measurement was performed in 10 ml of CF and CFG nanoparticles dispersion (2 mg ml^{-1}) in 0.05% w/v PAA gel medium. The *Hf* factor used for hyperthermia applications in this work was estimated to be 4.19 $\times$ 10^9 Am^{-1} s^{-1}, which is comparatively within the threshold limit [41]. The figures 8(a) and (b) shows the heating curve and specific absorption rate of CF and CFG nanoparticles. It was observed that the heating efficiency and specific absorption rate of the cobalt ferrite increases monotonically with the increase in the dopant (Gd^{3+}) concentration upto $x \leqslant 0.24$, whereas it decreases with further increase due to the evolution of the gadolinium hydroxide which possess larger particle size and reported to exhibit very weak magnetization. The increase in the specific absorption rate of CF and CFG ($x \leqslant 0.24$) nanoparticles is mainly due to the increase in particle size and increased poly-dispersivity [54]. The increase in SAR can also be explained by the decrease in the strength of magnetic interactions and anisotropy constant of CF and CFG nanoparticles [54].

Conclusion

The morphological, structural, crystallographic properties were investigated and found that the substitution of the gadolinium over 0.24 M showed an impure phase of gadolinium oxide. Magnetic measurement revealed the change in the direction of magnetization towards easy axis with increasing dopant concentration. The relaxation studies showed significant change in r_1 and r_2 relaxivities with respect to the gadolinium concentration. The hyperthermia efficiency has been greatly increased with the incorporation of gadolinium atom, makes them a potential candidate for Magnetic hyperthermic applications. The incorporation of these magnetic nanoparticles into drug loaded polymeric nanoparticles could help to enhance the site targeting, sensitivity of chemotherapeutic dose and provide adjuvant therapy along with chemotherapy.

Acknowledgments

Authors are grateful to the Department of Biotechnology, Government of India (Sanction order No. BT/PR8910/NNT/28/684/2013) for their support, Authors also thank Nanotechnology Research Center, SRM Institute of Science and Technology for providing the facilities.

ORCID iDs

Jaison D https://orcid.org/0000-0002-7176-357X
Meher Abhinav E https://orcid.org/0000-0002-8210-8255
Gopalakrishnan Chandrasekaran https://orcid.org/0000-0003-0971-3798

References

[1] Baronzio G F and Dieter Hager E 2006 Hyperthermia in cancer treatment: a primer *Medical Intelligence Unit* (Berlin: Springer)
[2] Brown S T and Fiering S 2014 Local tumour hyperthermia as immunotherapy for metastatic cancer *Int. J. Hyperth.* **30** 531–9
[3] Hervault A and Thanh N T K 2014 Magnetic nanoparticle-based therapeutic agents for thermo-chemotherapy treatment of cancer *Nanoscale* **6** 11553–73
[4] Dutz S and Hergt R 2013 Magnetic nanoparticle heating and heat transfer on a microscale: basic principles, realities and physical limitations of hyperthermia for tumour therapy *Int. J. Hyperth.* **29** 790–800
[5] Abinsa H F and Daud W M A W 2017 Review on magnetic nanoparticles for magnetic nanofluid hyperthermia application *Mater. Des.* **123** 174–96
[6] Mahmoudi K, Bouras A, Bozec D, Ivkov R and Hadjipanayis C 2018 Magnetic hyperthermia therapy for the treatment of glioblastoma: a review of the therapy's history, efficacy and application in humans *Int. J. Hyperth.* **34** 1316–28
[7] Kafrouni L and Savadogo O 2016 Recent progress on magnetic nanoparticles for magnetic hyperthermia *Progress in Biomaterials* **5** 147–60
[8] Haris M, Yadav S K, Rizwan A, Singh A, Wang E, Hariharan H and Marincola F M 2015 Molecular magnetic resonance imaging in cancer *Journal of Translational Medicine* **13** 313
[9] Menezes G L, Knuttel F M, Stehouwer B L, Pijnappel R M and van den Bosch M A 2014 Magnetic resonance imaging in breast cancer: a literature review and future perspectives *World Journal of Clinical Oncology* **5** 61–70
[10] Price P M, Mahmoud W E, Al-Ghamdi A A and Bronstein L M 2018 Magnetic drug delivery: where the field is going *Frontiers in Chemistry* **6** 619
[11] Vangijzegem T, Stanicki D and Laurent S 2019 Magnetic iron oxide nanoparticles for drug delivery: applications and characteristics *Expert Opinion on Drug Delivery* **16** 69–78
[12] Malik A, Butt T T, Zahid S, Zahid F, Waquar S, Rasool M, Qazi M H and Qazi A M 2017 Use of magnetic nanoparticles as targeted therapy: theranostic approach to treat and diagnose cancer *Journal of Nanotechnology* **2017** 1–8
[13] Achachelouei M F, Marques H K, Ribeiro da Silva C E, Barthes J, Bat E, Tezcaner A and Vrana N E 2019 Use of nanoparticles in tissue engineering and regenerative medicine *Frontiers in Bioengineering and Biotechnology* **7** 113
[14] Adedoyin A A and Ekenseair A K 2018 Biomedical applications of magneto-responsive scaffolds *Nano Res.* **11** 5049–64
[15] Ito A and Kamihira M 2011 Tissue engineering using magnetite nanoparticles *Prog. Mol. Biol. Transl. Sci.* **104** 355–95
[16] Tabi J K, Wilhelm C, Clement O and Gazeau F 2013 Cell labelling with magnetic nanoparticles: opportunity for magnetic cell imaging and cell manipulation *Journal of Nanobiotechnology* **11** 1–19
[17] Gu H, Xu K, Xu C and Xu B 2006 Biofunctional magnetic nanoparticles for protein separation and pathogen detection *Chem. Commun.* **37** 941–9
[18] Schwaminger S P, Blank-Shim S A, Scheifele I, Pipich V, Fraga-García P and Berensmeier S 2018 Design of interactions between nanomaterials and proteins: a highly affine peptide tag to bare iron oxide nanoparticles for magnetic protein separation *Biotechnol. J.* (https://doi.org/10.1002/biot.201800055)
[19] Cardoso V F, Francesko A, Ribeiro C, Bañobre-López M, Martins P and Lanceros-Mendez S 2017 Advances in magnetic nanoparticles for biomedical applications *Adv. Healthcare Mater.* **7** 1700845 1-35
[20] Moerland C P, van IJzendoorn L J and Prins M W J 2019 Rotating magnetic particles for lab-on-chip applications—a comprehensive review *Lab Chip* **19** 919–33
[21] Amiri M, Salvati-Niasari M and Akbari A 2019 Magnetic nanocarriers: evolution of spinel ferrites for medical applications *Advances in Colloid and Interface Sciences* **265** 29–44
[22] Thomas J, Thomas N, Girgsidies F, Beherns M, Huang X, Sudheesh V D and Sebastian V 2017 Synthesis of cobalt ferrite nanoparticles by constant pH co-precipitation and their high catalytic activity in CO oxidation *New J. Chem.* **41** 7356–63
[23] Hussain A, Abbas T and Niazi S B 2013 Preparation of $Ni_{1-x}Mn_xFe_2O_4$ ferrites by sol–gel method and study of their cation distribution *Ceram. Int.* **39** 1221–5
[24] Eom Y, Abbas M, Noh H Y and Kim C G 2016 Morphology-controlled synthesis of highly crystalline Fe_3O_4 and $CoFe_2O_4$ nanoparticles using a facile thermal decomposition method *RSC Adv.* **6** 15861–7
[25] Chen R, Christiansen M G, Sourakov A, Mohr A, Matsumoto Y, Okada S, Jasanoff A and Anikeeva P 2016 High-performance ferrite nanoparticles through nonaqueous redox phase tuning *Nano Lett.* **16** 1345–51
[26] Liu Y, Li J-J, Min F-F, Zhu J-B and Zhang M-X 2014 Microwave-assisted synthesis and magnetic properties of $Ni_{1-x}Zn_xFe_2O_4$ ferrite powder *J. Magn. Magn. Mater.* **354** 295–8
[27] Leonel L V, Barbosa J B S, Miquita D R, Fernandez-Outon L E, Oliveira E F and Ardisson J D 2018 Facile polyol synthesis of ultrasmall water-soluble cobalt ferrite nanoparticles *Solid State Sci.* **86** 45–52
[28] Yadav R S, Kuritka I, Vilcakova J, Havlica J, Kalina L, Urbanek P, Machovsky M, Skoda D, Masar M and Holek M 2018 Sonochemical synthesis of Gd^{3+} doped $CoFe_2O_4$ spinel ferrite nanoparticles and its physical properties *Ultrasonics—Sonochemistry* **40** 773–83
[29] Pillai V and Shah D O 1996 Synthesis of high-coercivity cobalt ferrite particles using water-in-oil microemulsions *J. Magn. Magn. Mater.* **163** 243–8

[30] Allaedini G, Tasirin S M A and Aminayi P 2015 Magnetic properties of cobalt ferrite synthesized by hydrothermal method *International Nano Letters* **5** 183–6
[31] Khorrami S A and Manuchehri Q S 2013 Magnetic properties of cobalt ferrite synthesized by hydrothermal and Co-precipitation methods: a comparative study *Journal of Applied Chemical Research* **7** 15–23
[32] Peng J, Hojamberdiev M, Xu Y, Cao B, Wang J and Wu H 2011 Hydrothermal synthesis and magnetic properties of gadolinium doped $CoFe_2O_4$ nanoparticles *Journal of Magnetism Magnetic Materials* **323** 133–8
[33] Shi Z, Sun L, Liu K, Zhang Y, Wang W and Jiang W 2019 Two-step hydrothermal synthesis of well-dispersed $(Na_{0.5}Bi_{0.5})TiO_3$ spherical powders *J. Nanomater.* **4768069** 1–8
[34] Thiesen B and Jordan A 2008 Clinical applications of magnetic nanoparticles for hyperthermia *Int. J. Hyperthermia.* **24** 467–74
[35] Hergt R, Dutz S, Müller R and Zeisberger M 2006 Magnetic particle hyperthermia: nanoparticle magnetism and materials development for cancer therapy *J. Phys. Condens. Matter* **18** S2919
[36] Fortin J P, Wilhelm C, Servais J, Ménager C, Bacri J-C and Gazeau F 2007 Size-sorted anionic iron oxide nanomagnets as colloidal mediators for magnetic hyperthermia *JACS* **129** 2628–35
[37] Levy M, Wilhelm C, Siaugue J-M, Horner O, Bacri J-C and Gazeau F 2008 Magnetically induced hyperthermia: size-dependent heating power of γ-Fe_2O_3 nanoparticles *Journal of Physics. Condensed Matter: An Institute of Physics Journal* **20** 204133
[38] Mazario E, Menendez N, Herrasti P, Canete M, Connord V and Carrey J 2013 Magnetic hyperthermia properties of electrosynthesized cobalt ferrite nanoparticles *J. Phys. Chem.* **117** 11405–11
[39] Virlan C, Bulai G, Caltun O F, Hempelmann R and Pui A 2016 Rare earth metals' influence on the heat generating capability of cobalt ferrite nanoparticles **42** 11958–65
[40] Hergt R and Dutz S 2007 Magnetic particle hyperthermia—biophysical limitations of a visionary tumour therapy *J. Magn. Magn. Mater.* **311** 187–92
[41] Hergt R, Hiergeist R, Zeisberger M, Glockl G, Weitschies W, Ramirez P, Hilger I and Kaiser W A 2004 Enhancement of AC-losses of magnetic nanoparticles for heating applications *J. Magn. Magn. Mater.* **280** 358–68
[42] Liu F, Laurent S, Roch A, Elst L V and Muller R N 2013 Size-controlled synthesis of $CoFe_2O_4$ nanoparticles potential contrast agent for MRI and investigation on their size dependent magnetic properties *J. Nanomater.* **2013** 127
[43] Bersuker I B 2010 *Electronic Structure and Properties of Transition Metal Compounds: Introduction to the Theory* (New York: Wiley)
[44] Grundmann M 2006 *The Physics of Semiconductors: An Introduction Including Devices and Nanophysics* (Berlin Hieldelberg (New York): Springer)
[45] Berlin J 2011 Analysis of boron with energy dispersive x-ray spectrometry: advances in light element analysis with SDD technology *Imaging and Microscopy* **13** 19–21
[46] Devore T C and Gallaher T N 1979 The vibrational infrared spectrum of CoO *J. Chem. Phys.* **71** 474–5
[47] Ma J, La L T B, Zaman I, Meng Q, Luong L, Ogilvie D and Kuan H-C 2011 Fabrication, structure and properties of epoxy/metal nanocomposites *Macromol. Mater. Eng.* **296** 465–74
[48] Sheibly D W and Fowler M H 1966 *Infra-Red Spectra of Various Metal Oxides in the Region of 2 to 26 Microns* (Cleveland, Ohio: Lewis Research Center) pp. 1–62 National Aeronautics and Space Administration, Washington
[49] Li C, Liu H and Yang J 2015 A facile hydrothermal approach to the synthesis of nanoscale rare earth hydroxides *Nanoscale Res. Lett.* **144**
[50] Gilleo M A 1960 Superexchange interaction in ferrimagnetic garnets and spinels which contain randomly incomplete linkages *J. Phys. Chem. Solids* **13** 33–9
[51] Lin Y-Q, Li J, Liu X-D, Zhang T-Z, Wen B-C, Zhang Q-M and Miao H 2010 Saturation magnetization and law of approach to saturation for self-formed ionic ferrofluids based on $MnFe_2O_4$ nanoparticles *Chin. J. Chem. Phys.* **23**
[52] Moskowitz B M 1991 Hitchhiker's guide to magnetism. Environmental Magnetism workshop, Institute for Rock Magnetism, www.magneticmicrosphere.com
[53] Santra S, Jativa S D, Kaittanis C, Normand G, Grimm J and Perez J M 2012 Gadolinium-encapsulating iron oxide nanoprobe as activatable NMR/MRI contrast agent *ACS Nano* **6** 7281–94
[54] Munoz-Menendez C, Leboran I C, Baldomir D, Chubykala-Fesenko O and Serantes D 2015 Role of size polydispersity in magnetic fluid hyperthermia: average versus local infra/over-heating effects *Phys. Chem. Chem. Phys.* **17** 27812–20